PFC/JA-84-42

PARTICLE CONFINEMENT AND THE ANOMALOUS DOPPLER INSTABILITY DURING COMBINED INDUCTIVE AND LOWER-HYBRID CURRENT DRIVE

S.C. Luckhardt, K-I. Chen, M.J. Mayberry,
M. Porkolab, Y. Terumichi,† G. Bekefi,
F.S. McDermott, and R. Rohatgi

Plasma Fusion Center and Research Laboratory of Electronics
Massachusetts Institute of Technology
Cambridge, Massachusetts 02139

December 1984

†Permanent address: Department of Physics, Kyoto University, Kyoto 606, JAPAN

ABSTRACT

Increases in average density have been observed during lower-hybrid current drive experiments (LHCD) on the Versator II tokamak, and on other LHCD experiments where inductive-ohmic and lower-hybrid current drive are combined. In the present experiments it is found that this density increase is the result of an improvement in global particle confinement time, τ_p, in comparison to purely ohmic discharges with similar plasma parameters. Furthermore, it is found that the improved confinement occurs only when the anomalous doppler relaxation instability of the anisotropic high energy electron tail is stabilized during LHCD.

†Permanent address: Department of Physics, Kyoto University, Kyoto 606, JAPAN

I. INTRODUCTION

In recent years considerable effort has been directed toward understanding lower-hybrid current drive in tokamaks. Lower-hybrid current drive alone or in combination with current drive by the inductive or ohmic heating electric field has been shown to be an effective method of efficiently maintaining, or ramping-up, the current in tokamak discharges.[1-4] However, relatively little attention has been given as yet to the questions of particle and energy confinement in lower-hybrid driven tokamak discharges. The density behavior, in particular, has been found to be anomalous in experiments where lower-hybrid current drive is introduced into quasi-steady ohmically driven discharges. It is generally observed that the plasma density tends to increase during the RF pulse.[1,5-7] In principle, such density behavior could result from additional ionization of hydrogen or impurity atoms, or from an increase in the particle confinement time of the discharge. In the present experiments the ionization and confinement behavior of discharges with inductive and combined inductive and lower-hybrid current drive is investigated and it is shown that the density increase is due to improved particle confinement.

Our experiments have been carried out in comparatively low density plasmas ($\bar{n}_e < 6 \times 10^{12} cm^{-3}$) where lower-hybrid current drive is most efficient for our source frequency of 800 MHz. In this low density regime inductively driven discharges possess a nonthermal runaway electron tail component and since the earliest tokamak experiments this type of discharge has been known to exhibit a relaxation instability of the electron tail. This instability, the anomalous doppler tail mode,[8-13] is driven by the velocity anisotropy of

the tail ($T_{\parallel} > T_{\perp}$). When the mode is unstable, a spectrum of unstable waves is generated and a fraction of the high energy tail electrons are scattered in pitch-angle by collective interaction with the waves. This instability manifests itself in experiments by enhanced cyclotron emission, x-ray bursts, and relaxation oscillations of the loop voltage, plasma current, and coincident bursts of RF noise. The application of lower-hybrid current drive to inductively driven discharges has been found to lengthen the period of the relaxation oscillations[14], and under some conditions the mode can be suppressed throughout the RF pulse. In fully RF driven discharges with constant current and $V_{loop} = 0$ the relaxation oscillations also can be stable[15-17,25,26]. In the present paper the suppression of the anomalous doppler mode and the particle confinement behavior during current drive are shown to be related.

The experiments were done on the Versator II tokamak device. The device parameters were: $R_0 = 40$ cm, $a = 13$ cm, $B_0 = 10\text{-}15$ kG, and $I_p = 30\text{-}40$ kA. Lower-hybrid waves were coupled into the Versator II plasma by means of a four waveguide phased array coupler made of carbon coated 304 L stainless steel. The individual waveguides had a 1 cm opening, a 20.8 cm height, and a wall thickness of 0.19 cm, and the power spectrum of the array as a function of wave number was peaked at $N_{\parallel}=ck_{\parallel}/\omega=6$ for relative phasing between waveguides of $\Delta\phi = 90°$. The source frequency was 800 MHz and the total power available was 100 kW. In the ohmic phase of the tokamak discharges the plasma density was controlled by a programmable gas feed system employing a piezoelectric puff valve. The vacuum chamber wall and limiter material was 304 L stainless

steel; impurities and recycling of neutrals were controlled by deposition of titanium on the vacuum chamber walls prior to each experimental run.

The following procedure was used in our experiments: quasi-steady plasma conditions were produced in an inductively driven initial phase of the discharge, then the RF power source was pulsed driving an additional RF current for a time which is long compared to the particle confinement time. This procedure allows the confinement before and during the RF pulse to be directly compared on the same shot.

II. DENSITY AND IONIZATION BEHAVIOR

The basic density phenomena under investigation occured, as shown in Fig. 1, when RF power was introduced into the ohmic discharge. The typical behavior of the density in the initial ohmic phase of the discharge was controlled by external hydrogen gas feed. In the case shown in Fig. 1 the initial gas puff raised the average density to $4.4 \times 10^{12} cm^{-3}$. After the gas feed was shut off the plasma density began to decay. When RF power was applied so as to drive current, the density decrease was arrested and the density began to increase. After the end of the RF pulse the density decayed rapidly. The Abel inverted 4mm interferometer data indicates that the density profile became somewhat more peaked during the RF pulse; this peaking is evident in Fig. 1b. The total number of electrons obtained from spatial integration of the spatial density profile, $N = 4\pi^2 R_o \int_o^a rdrn(r)$, increased during the RF pulse and approximately followed the behavior of $\bar{n}$. However, the time evolution of N

did not follow that of $\bar{n}$ identically because of profile changes. This density behavior was typical of cases where the lower-hybrid coupler was phased so as to launch traveling waves in the electron ohmic drift direction, i.e., the current drive direction. When the coupler phasing was reversed so as to launch waves in the anticurrent drive direction, $\Delta\phi = -90°$, no density increase was seen.

In general, increases in plasma density and total particle number may result from three possible causes: (1) increased ionization of hydrogen, (2) increased ionization of impurities, and (3) improved particle confinement. The first two possibilites were carefully explored and eventually rejected. The hydrogen and common impurity line emissions were surveyed using visible and UV instruments, and the behavior of the hydrogen and impurity ionization sources were found to decrease or remain unchanged during the density rise as shown below.

The ionization rates of hydrogen were inferred from H_α line emission. The H_α emissivity is proportional, over a wide range of plasma conditions, to the volumetric hydrogen ionization rate.[18] The hydrogen line emission was monitored, both with a ½-m visible monochromator, and with a small photodiode detector which viewed the plasma through an H_α line interference filter. The small H_α detector was easily movable between shots from one viewing port location to another. Using this detector the H_α behavior was monitored at five toroidal locations. Representative signals of this H_α survey are shown in Fig. 2a. The signals shown were all taken during a single run. Under fixed experimental conditions, the time dependence and amplitude of the

H_α signals were well reproducible from shot-to-shot. Interestingly, the monitored H_α emission generally decreased during the LHCD density rise and remained, for the duration of the RF pulse, at levels typically 10-30% lower than the purely ohmic case. Thus, during the RF pulse the ionization rate decreased, even though the density increased. In general, at the end of the RF pulse the H_α signals increased rapidly. This behavior was in contrast to the effects of gas puffing in the purely ohmic phase of the discharge. As seen in Fig. 2a the density rise caused by the initial hydrogen gas puff was accompanied by a significant rise in H_α brightness at all toroidal locations, with the largest increase occuring at locations nearest the puff valve.

The decreases in the hydrogen ionization rates during the RF pulse evident from the H_α signals in Fig. 2a are expected if indeed the bulk particle confinement was improved during the RF pulse. When the bulk particle confinement improves, the global loss rate of particles from the plasma must decrease and consequently the flux of particles to the chamber walls decreases. Such a reduction in particle flux to the walls then causes a reduction in the recycling rate of neutral hydrogen from the walls which is observable as a decrease in the H_α signal level. The observation of reduced H_α signals during the RF pulse is therefore consistent with an improvement in the global particle confinement time.

It is noteworthy that when additional H_2 gas was supplied by opening the gas puff valve during the RF pulse, very large increases in density were obtained in comparison to puffing during the ohmic phase. This increase was sometimes large enough to cause a loss of radial equilibrium position control

of the plasma. Also, gas puffing during the RF pulse in some cases caused the density to increase above the density threshold for efficient current drive with the 800 MHz power source, $\bar{n} = 6 \times 10^{12} cm^{-3}$[1]. In view of the sensitivity of the plasma to gas puffing during current drive, most data were taken with the gas puff valve closed during the RF pulse. The hydrogen ionization rates were maintained by recycling of neutral hydrogen from the vacuum chamber walls. With refined gas feed rate control and equilibrium position control, gas puffing experiments during the RF pulse should be possible.

The possibility of RF induced breakdown must also be considered as a potential source of ionization; RF electric fields in the range of 1kV/cm can occur at the end of the waveguide coupling structure. Such electric fields may cause significant hydrogen ionization under breakdown conditions. To investigate this possibility, the H_α detector was used to view the waveguide coupler directly. In these experiments the RF coupler was mounted in a top port, above the plasma, and the H_α detector viewed the entire waveguide area from a bottom port located directly below the RF coupler. As shown in Fig. 2a, the H_α emission from the RF port location did not increase during the RF pulse; thus RF induced ionization was not occurring in these cases, and cannot be the source of the plasma density increase.

It is important to determine the spatial extent of the ionization source region in the plasma in these low density conditions to ascertain that localized sources of ionization were not neglected in the H_α survey. In high density tokamak operation, the highest ionization rates are normally found near the gas feed port and the limiters, and can be localized in a relatively

narrow region near the edge of the plasma.[19] In the low density regime the ionization mean free path is longer so the spatial extent of the ionization region is expected to be more diffuse. The radial extent of the ionization region was obtained in the present experiments by horizontal and vertical scans of the collimated H_α detector. These spatial scans indicated that the hydrogen ionization was not strongly localized near the edge, but had a relatively flat profile with a broad maximum at r = 8-10 cm.

The measurement of the net hydrogen ionization rate was possible in these discharges because of the relatively weak dependence of the ionization source on radial and toroidal position. In Fig. 2a the H_α signal levels at the various toroidal locations are seen to be similar during the RF pulse; in contrast, during the initial ohmic phase the H_α signal from the gas puff port location is typically a factor of 2-3 higher than at the other locations. Because the H_α emission was not highly localized, the signals from the toroidal locations monitored during the H_α survey were taken as representative of the global H_α behavior.

The behavior of the nonhydrogenic species, e.g., oxygen, carbon, nitrogen, etc. was also monitored by means of the visible and VUV monochromators. As evident in Fig. 2b, the chord brightness of typical impurity lines decreased or remained unchanged during the RF pulse. These measurements imply that there was not any significant increase in the influx of impurity components during current drive, at least at the RF power levels of interest in these experiments. This result is in contrast to experiments at high power density where impurity generation can be a serious problem.[20] An influx of

impurity atoms sufficient to cause the observed large electron density increase would certainly cause a detectable increase of line radiation. From these impurity measurements, and the H_α survey, it is concluded that there was no significant global increase in ionization of hydrogen or impurity species during the injection of RF power, and hence increase must have been caused by improved particle confinement during the RF current drive phase of the discharge.

III. PARTICLE CONFINEMENT

The qualititive conclusion arrived at the preceding section, that the particle confinement time, τ_p, increased during RF current drive will be made more quantitative in this section. An analysis of the time evolution of the global particle balance in the discharge was carried out, and the relative magnitude of the particle confinement time during the ohmic and current drive phases of the discharge was determined. The global particle confinement time is defined by the particle balance equation:

$$\tau_p = \frac{N}{S - dN/dt} \tag{1}$$

where N is the total number of electrons in the discharge (obtainable from spatial integration of the density profile data), S is the total ionization source, and τ_p is the global particle confinement time. The quantities N and dN/dt entering the definition of τ_p are easily determined from spatially scanning microwave interferometer measurements and Abel inversion. Direct measurement of the total ionization source, S, is more difficult. At the

temperature and density typical in these discharges, the H_α line emissivity is approximately proportional to the volumetric hydrogen ionization rate, and, in principle, absolute intensity measurements of the H_α line emission from the entire toroidal plasma would be necessary to obtain the total ionization source S. This is not possible, however, due to the inevitable limitations of port access to the vacuum chamber. Fortunately, the desired information about S is obtainable owing to the fact that in these low density discharges the ionization region is diffuse and relatively uniform toroidally, at least during the RF pulse.

The H_α signals were surveyed at a number of toroidal locations and were found to have similar time dependences during the RF pulse, as is evident in Fig. 2a. Thus a single H_α signal may, in fact, be taken as representative of the time dependence of S, or equivalently, signals from many port locations may be averaged. The source function is obtained using the equation:

$$S = S_0 \frac{\langle H_\alpha(t) \rangle}{\langle H_{\alpha 0} \rangle} \tag{2}$$

where S_0 is the source function at some initial time $t = t_0$ before the RF pulse, $\langle H_\alpha (t) \rangle$ is the H_α brightness averaged over all toroidal locations, and $H_{\alpha 0}$ is the initial H_α brightness at $t=t_o$. The time dependence of S is contained in the quantity $\langle H_\alpha (t) \rangle$. Only the initial normalization of $S = S_0$ at $t = t_0$ remains to be determined.

In the following analysis the initial normalization of S is obtained by choosing an initial value of $\tau_p = \tau_o$ at $t=t_0$; this choice, together with the measured values of N and dN/dt determine S_0 through Eq. (1). This procedure is justified since the quantity of interest is the relative increase in the ratio τ_p/τ_o during the RF pulse, and as will be shown below, this ratio turns out to be relatively insensitive to the numerical value of τ_0 chosen. With S_0 determined by the choice of τ_0, the subsequent time evolution of S is obtained from the H_α signals, thus the time evolution of S and hence τ_p can be calculated using Eqn.s, (1) and (2).

An example of the evolution of τ_p during the RF pulse is shown in Fig. 3. The initial value of τ_p was chosen to be τ_0=0.5 milliseconds which is consistent with the observed density evolution in the initial ohmic phase of the discharge. During the RF pulse, τ_p increased rapidly for a 3 millisecond interval, then increased more slowly to a maximum value of 1.2 millisecond at the time of maximum density. As the density began to decay τ_p slowly decreased, and when the RF was shut off τ_p decreased rapidly on a sub millisecond time scale. The evolution of τ_p shown in Fig. 3 is typical of cases where RF current is driven with sufficiently high RF power levels. The RF power threshold at which this confinement increase occurs will be discussed in the next section.

Of course, the magnitude of τ_p obtained above is dependent on the initial value, $\tau_p = \tau_0$; however, the result that τ_p approximately doubles during the RF pulse is relatively insensitive to the numerical value of the confinement time τ_0 in the initial ohmic discharge. This may be seen by

rewriting the particle balance equation in terms of the ratio of the confinement time during the RF pulse at peak density, $\tau_p = \tau_1$, to the initial confinement time τ_0. The ratio of confinement times is given by:

$$\frac{\tau_1}{\tau_0} = \frac{N_1 S_0}{N_0 S_1}\left(1 + \frac{\tau_0}{N_0}\frac{dN_0}{dt}\right)^{-1} \qquad (3)$$

where the quantities with subscript zero refer to the initial time t_0 before the RF pulse, and those with subscript one refer to the later time t_1 when dN/dt = 0 during the RF pulse. For the data shown in Fig. 3 the ratio of confinement times is $\tau_1/\tau_0 = 2.32$ for τ_0 = 0.5 millisecond, and this ratio varies by only $\pm$ 10% for $0.1 < \tau_0 < 1.0$ millisecond. Therefore, the factor of 2.3 increase in confinement during the RF pulse for the data analyzed in Fig. 3 may be stated with confidence.

Using a simple extension of the global particle confinement equation, we can also calculate the reduction in particle loss rate during the transition from the ohmic phase to the improved confinement phase. The loss rate during the improved confinement phase will be denoted by R_0; during the RF pulse we have $N/\tau_p = R_0$. During the ohmic phase some additional losses are present and this additional loss rate is denoted by R'. In the ohmic phase

$$\frac{N}{\tau_p} = R_0 + R'. \qquad (4)$$

The loss term R' represents a particle loss channel which is operative during the ohmic phase and inoperative during the improved confinement phase. In this model, the effect of the RF is simply to eliminate the loss term R', leaving the term R_0 unchanged. The ratio of the loss terms from the above equations is

$$\frac{R'}{R_o} = \frac{\tau_1 N_o}{\tau_o N_1} - 1 \qquad (5)$$

The quantities with subscript zero refer to a time t_0 before the RF pulse and those with subscript one refer to a time t_1 during the RF pulse. For the data in figure 3 we have t_0 = 17.5 milliseconds, $N_0 = 3.1 \times 10^{17}$ particles and t_1 = 27.5 milliseconds, $N_1 = 4.0 \times 10^{17}$ particles. The ratio τ_1/τ_0 was found above to be 2.3. So the ratio of the loss terms in this case is $R'/R_0 = 0.8$.

Hence, during the improved confinement phase the particle loss rate decreased by the factor $R_0/(R_0 + R') = .55$. The loss channel R', accounting for approximately 45% of the total particle losses during the ohmic phase, has been eliminated by the application of lower-hybrid current drive.

Of course, modeling the transport of particles by the global particle balance is only the simplest approach to the problem. In view of the peaking observed in the density profile during the RF pulse, Fig. 1b, it may be possible that the local transport rate near the magnetic axis is reduced by the action of the RF. Such peaking would occur if the outward particle transport in the central core of the plasma was reduced. Detailed modeling of the spatial density profile will require numerical solution of the relevant

transport equations. Even such modeling may not allow a unique determination of the diffusion coefficient in view of the apparent necessity of including both an anomalous diffusion coefficient dependent on the radial coordinate, and an anomalous inward particle flux.[21,22]

It also appears possible that the global energy confinement time, τ_E, may be affected by lower-hybrid current drive in the same way as the particle confinement. Central electron temperature measurements reported earlier[1], and approximate global power balance calculations give preliminary indications that the bulk energy confinement time, τ_E, may also have increased during the RF pulse; however, temperature profile data and radiative power loss measurements will be needed to confirm the behavior of τ_E during current drive.

IV. ANOMALOUS DOPPLER MODE

Tokamak discharges in regimes of sufficiently low density ($\omega_{pe} < \omega_{ce}$), as is well known, are typified by the appearance of suprathermal runaway electron tails.[8,23] The anisotropy of the resulting electron velocity distribution ($T_\parallel > T_\perp$) can drive the anomalous doppler instability, a characteristic relaxation instability in these discharges, which causes periodic oscillations in various monitored signals.[23] The experimental indications of this unstable mode include the following: enhanced non-thermal emission at the electron cyclotron frequency and its harmonics, bursts of hard x-ray emission from the limiter and chamber walls, enhanced perpendicular x-ray bremsstrahlung

radiation from the plasma, and bursts of RF radiation in the frequency range $\omega_{pi} \ll \omega < \omega_{pe}$[14,23,24].

In this section, it will be shown that the improved confinement behavior discussed in the previous sections is associated with the RF induced stabilization of this tail mode. The physical picture of this mode, put forward in reference 9, will briefly be recounted. The anisotropy of the electron distribution produced by the ohmic heating electric field can excite unstable electrostatic waves $\omega = \omega_{pe} k_{\parallel}/k$ through competition between Landau damping at $\omega = k_{\parallel} v_{\parallel}$ and growth at the anomalous doppler resonance, $\omega + \omega_{ce} - k_{\parallel} v_{\parallel} = 0$, where $k_{\parallel}$, and $v_{\parallel}$ are the wave number and electron velocity parallel to the magnetic field, ω_{ce} is the electron cyclotron frequency and ω_{pe} is the electron plasma frequency. In the doppler resonance interaction the wave effectively pitch-angle scatters the high energy electrons in the tail. The pitch-angle effect tends to increase the tail temperature perpendicular to the magnetic field, $T_{\perp}$, evolving the distribution function to a more isotropic state. After the anomalous doppler resonance produces sufficient pitch-angle scattering, a second stage of the instability occurs in which electrons which were bunched at lower $v_{\parallel}$ in the first stage excite an additional wave spectrum through Landau growth. The consequent quasi-linear diffusion then flattens the tail in the parallel direction. The final relaxed state of the electron distribution exhibits an extended tail in the parallel direction with a large perpendicular temperature. The steady state ohmic heating electric field then can accelerate electrons toward larger $v_{\parallel}$ values, eventually resulting in an unstable distribution again. This

process can repeat giving rise to the observed relaxation instability. This picture appears to give a good qualitative account of the features of this mode as observed in ohmic discharges.

When the toroidal current is generated by lower-hybrid waves the behavior of the tail mode will be modified by quasi-linear effects produced by the externally applied waves. In the experiments the immediately apparent effect of LHCD on the behavior of this mode was to increase the period between relaxation bursts compared to purely ohmic discharges.[14] Previously, the Versator II experiments have shown that the addition of sufficient electron cyclotron heating power could stabilize this mode[17], and in purely RF current sustained plasmas with $dI/dt = 0$, and $V_{loop} = 0$ the relaxation oscillations also can be stable[15,16,17,25,26] although at the end of the RF power pulse the tail mode may appear.[25]

In our experiments it was found that under conditions when sufficient lower-hybrid power was applied to the ohmic discharge, the relaxation mode was suppressed, as indicated by the absence of loop voltage oscillations, x-ray bursts, RF busts, etc.; note, however, that the measured loop voltage need not be necessarily zero. It is also found that this mode suppression is sensitive to small changes in plasma equilibrium position and impurity levels, and may be triggered by small changes in these quantities. Similar stabilization effects by LHCD have been reported in the T-7 tokamak experiments.[27] In the present paper our main interest is in the correlation of the RF suppression of the relaxation mode with the confinement increase during lower hybrid current drive so the details of the stability threshold of this mode, and its

dependence on various plasma parameters will not be treated in great detail.

A comparison between discharges where the mode was suppressed during current drive, and where a single mode burst occured is shown in Fig. 4. In Fig. 4a suppression of the tail mode during the RF pulse is evident. The loop voltage and hard x-ray signals are smooth and show no bursts until the end of the RF pulse at which time the mode activity again appears. The density and H_α emission are also smooth and indicate an increase of particle confinement during the RF pulse. With a small change of equilibrium conditions, however, a repeatable example of a single instability burst during the RF pulse was produced, as shown in Fig. 4b. In this case the characteristic x-ray burst and loop voltage spike occur at t = 9 milliseconds, as indicated by the marker arrow in Fig. 4b. In addition to the burst activity evident on loop voltage and x-ray emission signals the behavior of the density and H_α signals are also in clear contrast to the case without mode activity (Fig. 4a). After the initial density rise at the beginning of the RF pulse, the density decayed rapidly immediately after the mode burst at t=9 millisecond; and overall, the amount of density rise was reduced (Fig. 4b) in comparison to that of Fig. 4a. This decrease in the central chord density continued for approximately 1.0 millisecond, then $\bar{n}$ reached a minimum and began to increase again. In the one millisecond period following the mode burst $\bar{n}$ decreased by 10% while in the case, Fig. 4a, without the burst, $\bar{n}$ increased by 15% in this time interval. As shown in Fig. 4b, the H_α behavior was also correlated with the bursting activity. During the RF pulse a representative H_α signal initially decreased, dropping rapidly below the ohmic level signal in approximately 1

millisecond, then when the mode burst occured, Fig. 4b, the H_α signal increased sharply for a period of 0.5 milliseconds, reached a maximum, then slowly decreased over a 1.5 millisecond period. The H_α signal shown in Fig. 4b is typical of the H_α signals seen at all monitored toroidal locations during a mode burst. From the particle confinement analysis above it follows that the particle confinement time decreased during the approximately 1.5 millisecond period following the mode burst, then began to increase again.

At lower RF power levels when several mode bursts occured during the RF pulse, or with reversed coupler phasing, little or no density increase was seen as compared to the case of purely ohmic discharges. It is important to note that at low power or with reversed phasing the density does not drop below that of the ohmic discharge, indicating that the particle confinement time is comparable to the purely ohmic case.

In general, after the RF pulse ends large mode bursts were observed; this can be seen in Fig. 4a and b as a rapid loop voltage increase and hard x-ray increase. At this time the H_α signal increased and the density rapidly decreased indicating a rapid drop in τ_p after the RF is shut off. Hence, the rapid drop in confinement at the end of the RF pulse is also correlated with a mode burst. As noted above, and in reference 14 the tail mode was active throughout most of the ohmic phase of these discharges, occurring both before and after the RF pulse. In the ohmic phase the period between bursts was typically a few hundred microseconds, and consequently the bulk signals such as the loop voltage and hard x-ray emission showed a quasi-steady level which

represents a time average of the rapid individual bursts during this phase of the discharge. Individual bursts in this phase however, were easily detected as RF noise bursts on RF probes.[14] To summarize, these observations indicate clearly that the improved confinement is correlated with the stabilization of the tail mode relaxation oscillation during LHCD.

Further evidence for the connection between the tail mode and confinement is shown in Fig. 5 where the density, H_α signal level, and the number of mode bursts occurring during the RF pulse are shown as a function of applied RF power. First, it is evident from this data that the density increase, and H_α decrease occur at a threshold in RF power, P_{th} = 4kW. When the RF power was increased further, so that $P_{rf} > P_{th}$ the density and H_α levels became independent of RF power. This observation also reinforces the conclusion that the density increase was not due to RF coupler breakdown, which would tend to become more severe with increasing RF power levels. Also shown in Fig. 5 is the power dependence of the number of tail mode instability bursts occurring during the RF pulse, up to the time when the density and H_α signals are sampled. It is evident that the RF power threshold for the suppression of the mode bursts is the same as the power threshold for the improved confinement behavior. It should be noted that the absolute power level of this stabilization threshold depends on the detailed equilibrium conditions of the discharge; nevertheless, the correlation between the mode suppression and confinement improvement was always evident. If the particle confinement increase occurs as a consequence of the stabilization of the tail mode relaxation instability, this power threshold can be understood: the saturation of the particle confinement and density increase with RF power (see Fig. 5) is

a consequence of the fact that the tail mode is fully stabilized at power levels $P_{rf} > P_{th}$.

In experiments where the phasing of the waveguide coupler was reversed to $\Delta\phi = -90°$, the period of the mode bursts also increased compared to that of the ohmic discharge. However, the mode period remained short compared to the RF pulse duration and mode suppression throughout the RF pulse was not obtained at least to power levels up to 50 kW. Furthermore, there was no significant improvement in confinement with $\Delta\phi = -90°$.

In the experiments described so far the plasma density was maintained at levels below $\bar{n} = 6 \times 10^{12}cm^{-3}$ the density limit for efficient current drive with the 800 MHz RF power source.[1] When RF power was injected into discharges with $\bar{n} > 6 \times 10^{12}cm^{-3}$ no significant density increase was observed during the RF pulse, nor was there a decrease in H_α emission. Thus RF injection did not affect the confinement in discharges with density above the current drive density limit. It must also be noted that in ohmic discharges with densities above $\bar{n} = 6\text{-}7 \times 10^{12}cm^{-3}$ the tail mode activity is generally absent under normal Versator II operating conditions.

V. DISCUSSION OF RESULTS AND CONCLUSIONS

From the above data and analysis it is evident that the density and particle confinement increase observed during our current drive experiments occured under conditions when the anomalous doppler tail mode was suppressed by the initiation of RF current drive. Several questions naturally arise from

these experimental results. First, what is the mechanism which stabilizes the tail relaxation mode during RF current drive ; and second, why is the particle transport enhanced when the mode is unstable. We will discuss both questions briefly before presenting our conclusions.

The anomalous doppler mode is driven by the anisotropy of the electron tail, $T_{\parallel} >> T_{\perp}$. Linear stability analysis of this mode yields the growth rate

$$\gamma = \frac{\pi}{2}\,\omega_k\,\frac{\omega_{pe}^2}{k^2}\,\frac{\partial f(v_\parallel)}{\partial v_\parallel}\bigg|_{v_\parallel = \frac{\omega_k}{k_\parallel}} - \frac{\nu_{e-i}}{2} \qquad (6)$$

$$+ \frac{\pi}{8}\,\frac{\omega_{pe}^2}{k^2}\,\omega_k \int 2\pi v_\perp dv_\perp \left(\frac{k_\perp v_\perp}{\omega_{ce}}\right)^2 \left[-\frac{v_\parallel}{v_\perp}\,\frac{\partial f}{\partial v_\perp} + \frac{\partial f}{\partial v_\parallel}\right]_{v_\parallel = \frac{\omega_{ce}+\omega}{k_\parallel}}$$

as given by reference 9. Here $f = f(v_\parallel, v_\perp)$ is the two dimensional electron velocity distribution function, $\int d^3v f(v_\parallel, v_\perp) = 1$, $f(v_\parallel)$ is the one dimensional distribution function, $f(v_\parallel) = \int 2\pi v_\perp dv_\perp\ f(v_\parallel, v_\perp)$, $\omega_k = \omega_{pe} k_\parallel / k$, ω_{pe} is the electron plasma frequency, and ν_{e-i} is the electron ion collision frequency.

The first term represents Landau damping of the unstable wave, the second term is the effect of collisional damping and the final term is the effect of the anomalous doppler resonance, which causes the wave to grow. This mode can become unstable with a runaway electron distribution function for which the tail parallel temperature substantially exceeds the perpendicular temperature.[9] Application of external RF wave power can modify $f(v_\parallel, v_\perp)$ by quasi-linear diffusion, possibly leading to stabilization of the mode. For

example, in our earlier experiments electron cyclotron heating was applied to increase the perpendicular temperature of the tail and it was found that when sufficient EC power was applied the tail mode relaxation oscillations were suppressed[14].

In the present experiments quasi-linear diffusion caused by lower-hybrid waves causes transport of electrons to higher $v_{\parallel}$, and increased $T_{\parallel}$. Thus the lower-hybrid waves apparently increase the anisotropy of the electron distribution function, and this is a destabilizing influence rather than a stabilizing one. The anomalous doppler mode can be stabilized by increasing the tail perpendicular temperature, or by decreasing the number of tail electrons at high velocities, $v_{\parallel} = (\omega_{ce} + \omega)/k_{\parallel}$. Both of these effects can decrease the destabilizing term containing $\frac{\partial f}{\partial v_{\perp}}$ which appears in the growth rate of the mode. The mode can also be stabilized by increasing the value of $\partial f/\partial v_{\parallel}$ at the Landau resonance, $v_{\parallel} = \omega/k_{\parallel}$. Further analysis of the quasi-linear equations such as in reference 31 will be needed to determine which of the above effects, if any, are responsible for our observations that the application of lower-hybrid power can stabilize the relaxation mode.

In several current drive experiments, under some conditions it was observed that the hard x-ray emission from the chamber walls was reduced during the RF pulse[1,5,15,25,30], see also Fig. 4a. This reduction in hard x-ray emission is surprising since the application of RF power tends to increase the number of high energy tail electrons in the plasma. However, this decreased x-ray emission, and hence decreased loss rate of fast electrons to the chamber walls and limiter may be a consequence of the RF stabilization

of the tail mode. During the ohmic phase of the discharge before application of RF power the mode bursting can be frequent and in this case pitch angle scattering of the fast tail electrons by the anomalous doppler resonance can result in trapping of a fraction of these electrons in the local magnetic mirrors present between toroidal field coils. As shown clearly in the TFR experiments[23] the mode activity in the ohmic discharge results in rapid periodic dumps of fast electrons to the wall at locations between toroidal field coils. Thus the mode activity can lead to enhanced losses of the high energy tail electrons. Clearly then, stabilization of the tail mode by lower-hybrid current drive would eliminate this fast electron loss process resulting in a reduced flux of fast electrons onto the walls and limiters. This mechanism may explain our observations of a decrease in the wall and limiter hard x-ray flux during the RF pulse.

Now the question of the mechanism responsible for the evident connection between the tail mode activity and particle confinement will be discussed. It is evident that the tail mode itself causes a direct loss of a fraction of the high energy electrons, as seen for example, by the hard x-ray burst evident in Fig. 4b. In the case of purely ohmic discharges this fast electron loss process is well documented, for example in reference 23, and references contained therein. A potential explanation of the particle confinement change when the tail mode is stabilized is that the direct loss of fast electrons is reduced by application of lower-hybrid current drive. When the mode is stabilized by RF current drive a fast particle loss channel is eliminated possibly leading to the observed increases in τ_p when the mode is stabilized.

Now we will show that ripple losses of the fast electron component represents a loss process which is too small to account for the observed reduced confinement during the ohmic phase of the discharges in our experiments. Fast electrons which are lost due to tail mode activity will carry energy out of the discharge, and since the lost particles are very energetic[23], the mode activity causes an energy loss as well as a fast particle loss. Since the upper bound for the energy loss is the input ohmic heating power we can obtain an upper bound on the energy of the lost electrons. As shown in section III, the anomalous particle loss channel which is suppressed by the RF represents a particle loss rate approximately given by

$$R' = .8R_0 = .8\,\frac{N_{RF}}{\tau_p} \qquad (7)$$

In the data presented in Fig. 3 we find at t = 23 milliseconds, $N_{RF} = 4 \times 10^{17}$ particles and $\tau = 1.15$ milliseconds which yields $R' = 2.8 \times 10^{20}$ particles/sec, for the anomalous particle loss rate which the RF suppresses. If ripple trapping and loss of the fast electron component is responsible for this loss rate, a corresponding energy loss rate must result. This power loss is given by: $P_{loss} = \overline{E}_t R'$ where $\overline{E}_t$ is the average energy of the ripple lost electrons. Clearly, the ohmic heating input power is greater than P_{loss}, hence we have the following upper bound for $\overline{E}_t$: $\overline{E}_t < P_{OH}/R'$. In the case of the data presented in Fig. 4 the value of P_{OH} is 15kW, and with the above value of R' we find that $\overline{E}_t < 400$eV, which is actually comparable to the

bulk central electron temperature in our experiments. Thus the average energy of the particles lost through the anomalous particle loss channel denoted by R' must be less than 400eV. On the other hand the energy of the electrons lost during the tail mode burst due to ripple trapping is on the order of 10-100keV. Hence it can be concluded that the ripple loss of fast electrons during the anomalous doppler mode is not the main particle loss process needed to explain the observed improved particle confinement during lower-hybrid current drive. The direct loss of the tail particles cannot account for the observed decreases in bulk density, for example, in Fig. 4b, after a mode burst. We conclude that some other process is responsible for the observed behavior of the particle confinement time during RF current drive when the tail mode is stabilized.

Effects which may play a role in the bulk particle transport include: magnetic fluctuations induced by the rapid tail current and current profile changes which appear to occur during a mode burst (fluctuations in the poloidal magnetic field were observed in our experiments with Mirnov type pickup coils), current driven drift-wave-like fluctuations, and changes in the electrostatic potential profile of the plasma. Further experimental work will be needed to determine which if any of these effects is responsible for the particle confinement changes.

In conclusion, our experiments have shown that the density increase observed during combined inductive and lower-hybrid current drive is due to a significant increase in particle confinement time. Furthermore, this increased confinement occurs when the anomalous doppler tail mode is stabilized by the initiation of lower-hybrid current drive.

ACKNOWLEDGEMENTS

The authors would like to thank Earl Marmar and James L. Terry of the Alcator Group for the use of the H_α detector. This work was supported by the U.S. Department of Energy (contract DE-AC02-78ET-51013).

REFERENCES

1. S. C. Luckhardt, M. Porkolab, S. Knowlton, K-I. Chen, A. Fisher, F.S. McDermott, Phys. Rev. Lett. 48 152 (1982).
2. F. Jobes, J. Stevens, R. Bell, S. Bernabei, A. Cavallo, T.K. Chu, S. Cohen, B. Denne, P. Efthimion, E. Hinnov, W. Hooke, J. Hosea, E. Mazzucato, R. McWilliams, R. Motley, S. Suckewer, G. Taylor, J. Timberlake, S. von Goeler, R. Wilson, Phys. Rev. Lett. 52 1005 (1984)
3. S. Kubo, M. Nakamura, T. Cho, S. Nakao, T. Shimozuma, A. Ando, K. Ogura, T. Maekawa, Y. Terumichi, and S. Tanaka, Phys. Rev. Lett. 50 1994 (1983).
4. M. Porkolab, J.J. Schuss, B. Lloyd, Y. Takase, S. Texter, P. Bonoli, C. Fiore, R. Gandy, D. Gwinn, B. Lipschultz, E. Marmar, D. Pappas, R. Parker, and P. Pribyl, Phys. Rev. Lett., 53, 450 (1984).
5. K. Ohkubo, S. Takamura, and the JIPPT-II Group, Proceedings of the 3rd Joint Varenna-Grenoble International Symposium on Heating of Toroidal Plasmas, ed.s C. Gormezano, G.G. Leotta, E. Sindoni, EUR 7979EN, 2 543 (1982).
6. G. Tonon, G. Gormezano, C. Cardinalli, M. El Shaer, W. Hess, G. Ichtchenko, R. Maone, G. Melin, D. Moreau, G.W. Pacher, H.D. Pacher, F. Soeldner, and J.G. Wegrowe, Proceedings of the 3rd Joint Varenna-Grenoble International Symposium on Heating of Toroidal Plasmas, ed.s C. Gormezano, G.G. Leotta, E. Sindoni, EUR 7979EN, 2, 623 (1982).
7. K. Uehara and T. Nagashima, Proceedings of the 3rd Joint Varenna-Grenoble Symposium on Heating of Toroidal Plasmas, ed.s C. Gormezano, G.G. Leotta, E. Sindoni, EUR 7979EN, 2 485 (1982).

8. H. Knoepfel and D.A. Spong, Nuclear Fusion 19 785 (1979).

9. V.V. Parail and O.P. Pogutse, Nuclear Fusion 18 3, 303 (1978).

10. V.D. Shapiro and V.I. Shevchenko, Soviet Physics JETP 27 635 (1968).

11. B. Coppi, F. Pegoraro, R. Pozzoli, G. Rewoldt, Nuclear Fusion 16 309 (1976).

12. K. Molvig, M.S. Tekula, and A. Bers, Phys. Rev. Lett. 38 1404 (1977).

13. D. Choi and W. Horton, Plasma Physics 20 903 (1978).

14. S.C. Luckhardt, G. Bekefi, P. Bonoli, K. Chen, B. Coppi, R. Englade, A. Fisher, K. Hackett, S. Knowlton, M. Mayberry, F. McDermott, M. Porkolab, J. Levine, M. Read, V. Granatstein. Prodeedings of the 3rd Joint Varenna-Grenoble International Symposium on Heating of Toroidal Plasmas ed.s C. Gormezano, G.G. Leotta, E. Sindoni, EUR 7979EN, 2 529 (1982).

15. S. Bernaebei, C. Daughney, P. Efthimion, W. Hooke, J. Hosea, F. Jobes, A. Martin, E. Mazzucato, E. Meservey, R. Motley, J. Stevens, S. von Goeler, and R. Wilson, Phys. Rev. Lett. 49 1255 (1982).

16. M. Porkolab, J.J. Schuss, Y. Takase, S. Texter, B. Blackwell, C. Fiore, R. Candy, R.S. Granetz, M. Greenwald, D. Gwinn, B. Lipschultz, E.S. Marmar, S. McCool, D.S. Pappas, R.R. Parker, P. Pribyl, J.E. Rice, J.L. Terry, R. Watterson, S.M. Wolfe, S.F. Knowlton, S.C. Luckhardt, M. Porkolab, G. Bekefi, K-I. Chen, A. Fisher, K. Hackett, M.J Mayberry F.S. McDermott, R. Rohatgi, A. Bers, P.T. Bonoli, B. Coppi, R. Englade, V. Krapchev, A. Ram, R.E. Slusher, C.M. Surko, J.S. Levine, M.E. Read, V.L. Granatstein, Plasma Physics and Controlled Nuclear Fusion Research, 1 227, International Atomic Energy Agency, Vienna (1982).

17. J. Stevens, S. Bernabei, M. Bitter, F. Boody, N. Bowen, A. Cavallo, T.K. Chu, S. Cohen, P. Colestock, S. Davis, C. Daughney, F. Dylla, P. Efthimion, D. Herdon, E. Hinnov, W. Hooke, J. Hosea, J. Hovey, H. Hsuan, D. Hwang, D. Ignat, F. Jobes, R. Kaita, J. Lawson, A. Martin, E. Mazzucato, D. McNeill, S. Medley, E. Meservey, R. Motley, D. Mueller, D. Ruzic, J. Schivell, F. Schnabl, R. Schwartz, J. Strachan, S. Suckewer, S. von Goeler, and R. Wilson. Proceedings of the 3rd Joint Varenna-Grenoble International Symposium on Heating of Toroidal Plasmas, ed.s C. Gormezano, G.G. Leotta, E. Sindoni, EUR 7979EN, 2 455 (1982).

18. L. C. Johnson and E. Hinnov., J. Quant. Spectrosc. Radiat. Transfer. 13 333 (1973).

19. E.S. Marmar, J. Nuclear Materials 76 and 77 59 (1978).

20. M. Porkolab, B. Lloyd, J.J. Schuss, Y. Takase, S. Texter, R. Watterson, C. Fiore, R. Gandy, R. Granetz, M. Greenwald, P. Gwinn, B. Lipschultz, E. Marmar, S. McCool, D. Pappas, R. Parker, P. Pribyl, J. Rice, J. Terry, and S. Wolfe, S.C. Luckhardt, K.I. Chen, S.F. Knowlton, G. Bekefi, M.J. Mayberry, S. McDermott, M. Porkolab, R. Rohatgi, and Y. Terumichi, Proceedings of the 4th Joint Varenna-Grenoble International Symposium on Heating in Toroidal Plasmas, ed.s H. Knoepfel and E. Sindoni, EUR 9341 EN, 1 529, Rome Italy (1984).

21. B. Coppi, N. Sharky, Nuclear Fusion 21 1363 (1981).

22. Yu. N Dnestrovskii, S.V. Neudachen, G.V. Pereverzev, I.V. Kurchatov Institute of Atomic Energy Report #3690/6 (1982).

23. EQUIPE TFR Nuclear Fusion 16 473 (1976).

24. V.V. Alikaev, Yu. I. Arseni'ev, G.A. Bobrovskii, A.A. Kondrati'ev, K.A. Razumova, Sov. Phys. Tech. Phys. 20 322 (1975).

25. S. von Goeler, J. Stevens, C. Karney, S. Bernabei, M. Bitter, T.K. Chu, P. Efthimion, K. Hill, W. Hooke, F. Jobes, E. Mazzucato, E. Meservey, R. Motley, P. Roney, N. Sauthoff, S. Sesnic, G. Taylor, F. Tenney, E. Valeo, Proceedings of 5th Topical Conference on Radio Frequency Plasma Heating, University of Wisconsin, Madison, Wisconsin, paper B2, 96, (1983).

26. W. Hooke, Plasma Physics 26 133 (1984).

27. V.V. Alikaev, V.L. Vdovin, D.P. Ivanov, N.V. Ivanov, V.I. Il'in, A.M. Kakurin, A. Ya. Kislov, P.E. Kovrov, V.A. Kochin, P.P. Khvostenko, I.N. Khromkov, V.V. Chistyako, J. Datlov, F. Jacek, P. Klima, V. Kopecky, J. Preinhaelter, K. Jakubka, Plasma Physics and Controlled Nuclear Fusion Research, 2 153, International Atomic Energy Agency, Vienna (1982).

28. F. Troyon and F.W. Perkins, Proceedings of the Second Topical Conference on Radio Frequency Plasma Heating, Texas Tech University, Lubbock, Texas paper B4 (1974).

29. P.T. Bonoli and E. Ott, Phys. Fluids 25 359 (1982).

30. T. Yamamoto, T. Imai, M. Shimada, N. Suzuki, M. Maeno, S. Konoshima, T. Fujii, K. Uehara, T. Nagashima, A. Funahashi, and N. Fujisawa, Phys. Rev. Lett. 45 716 (1980).

31. C.S. Liu, V.S. Chan, D.K. Bhadra, R.W. Harvey, Phys. Rev. Lett. 48 1479 (1982).

FIGURES

1 a) Time dependence of the average density in a purely ohmic discharge (dashed curve) and a discharge with lower-hybrid current drive and ohmic drive combined (solid curve). Density profiles were taken at the times indicated by the arrows.

1 b) Density profiles at the times indicated in Fig. 1a. The error bar indicates an estimate of the maximal curve fitting error in the Abel inversion of the interferometric chordal data.

2 a) Time dependence of density and H_α brightness at various toroidal locations during gas puffing and RF current drive.

2 b) Chordal brightnesses of various impurity lines during RF current drive. FeII 259.9 nm, CIII 229.7 nm, OV 278.1 nm, CV 227.1 nm, and NVI 189.7 nm.

3. Time dependence of the total particle number, N, as obtained by spatial integration of the density profile data, dN/dt, and the total ionization source, obtained from H_α data, and the evolution of the global particle confinement time τ_p obtained from equation 1. The initial value of τ_p in the ohmic phase was taken to be τ_o = 0.5 millisecond.

4 a) Time dependence of density, H_α brightness, plasma current, loop voltage, hard x-ray emission, and RF power for a case with no tail mode bursting activity during the RF pulse.

4 b) Time dependence of signals for the case of a single tail mode burst occuring during the RF pulse at the time indicated by the marker arrows.

5. Dependence on RF power level of average density, H_α brightness during the RF pulse, and the number of tail mode instability bursts occuring during the RF pulse.

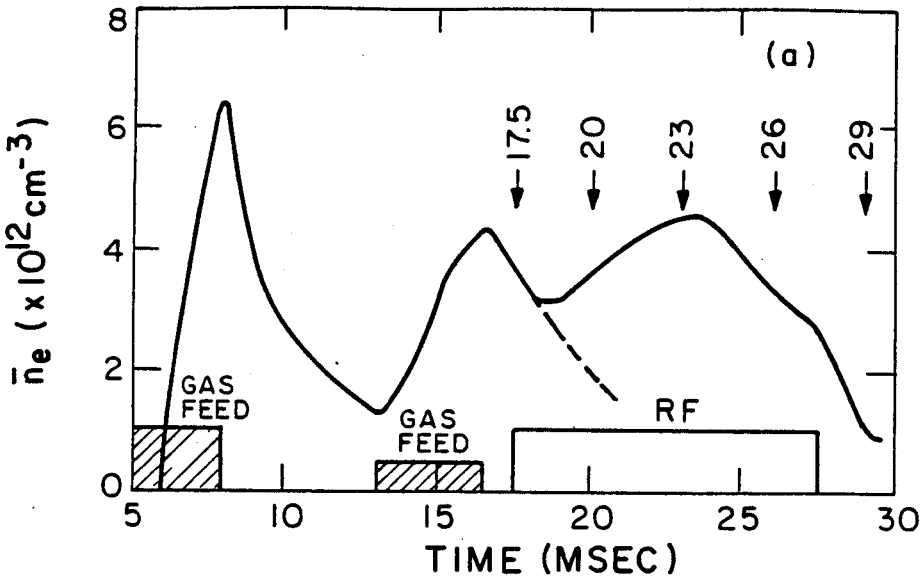
(a)
$\bar{n}_e$ ($\times 10^{12}$cm^{-3})
8
6
4
2
0
17.5
20
23
26
29
GAS FEED
GAS FEED
RF
5
10
15
20
25
30
TIME (MSEC)

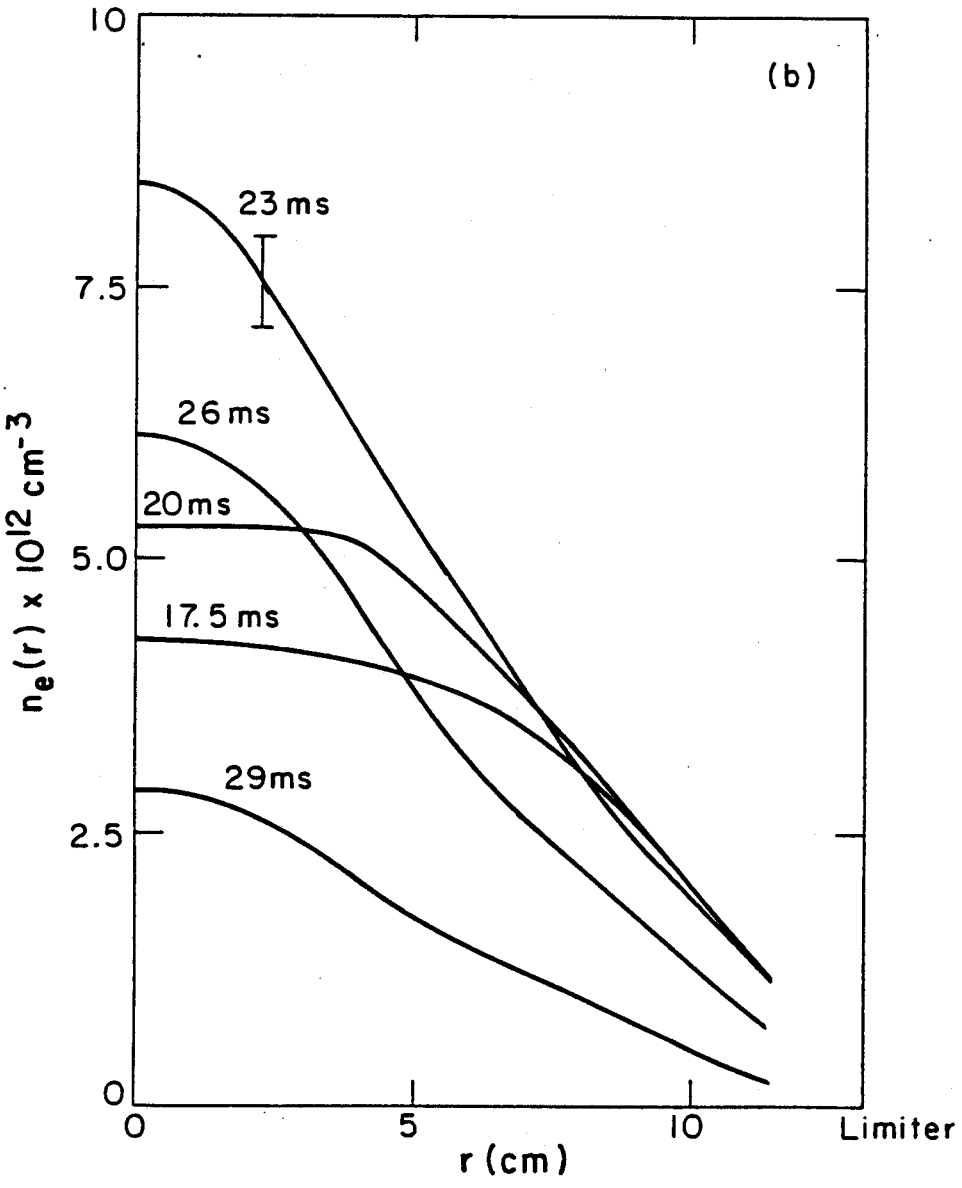
(b)
$n_e(r) \times 10^{12}$ cm^{-3}
10
7.5
5.0
2.5
0
23 ms
26 ms
20 ms
17.5 ms
29 ms
0
5
10
Limiter
r (cm)

FIG. 1

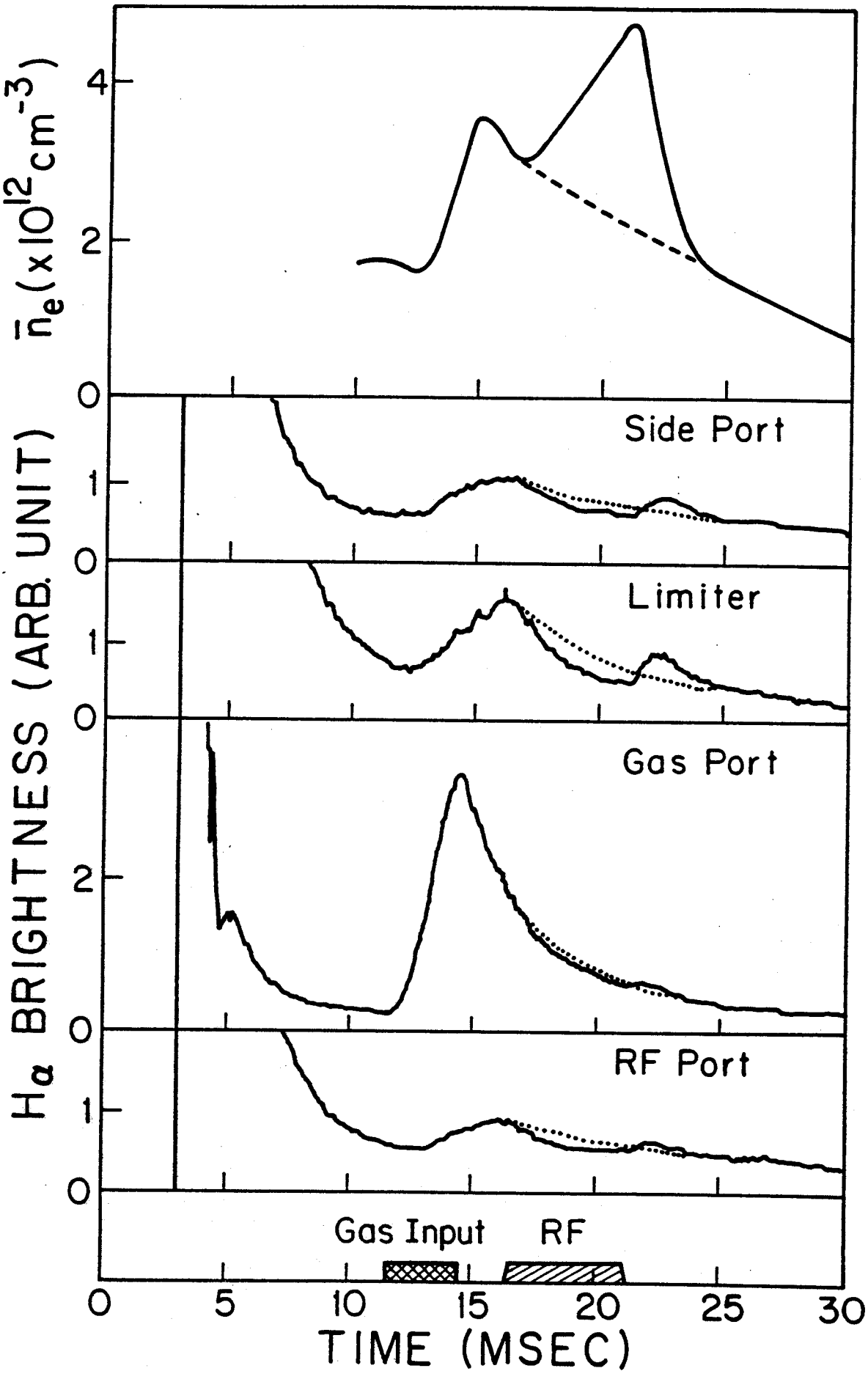
$\bar{n}_e (\times 10^{12} cm^{-3})$
4
2
0
H_α BRIGHTNESS (ARB. UNIT)
Side Port
Limiter
Gas Port
RF Port
1
2
Gas Input
RF
0
5
10
15
20
25
30
TIME (MSEC)

FIG. 2a

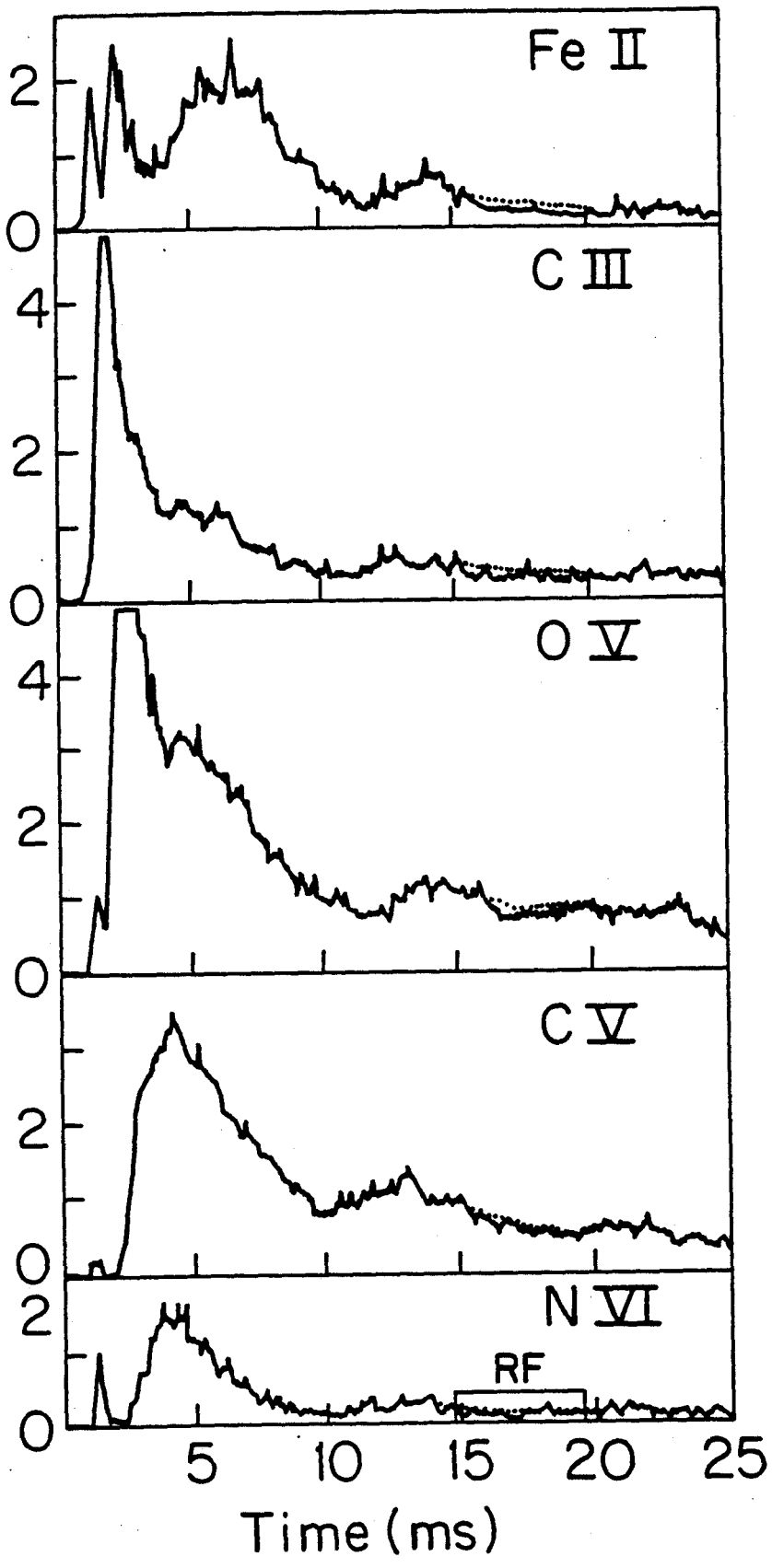

FIG. 2b

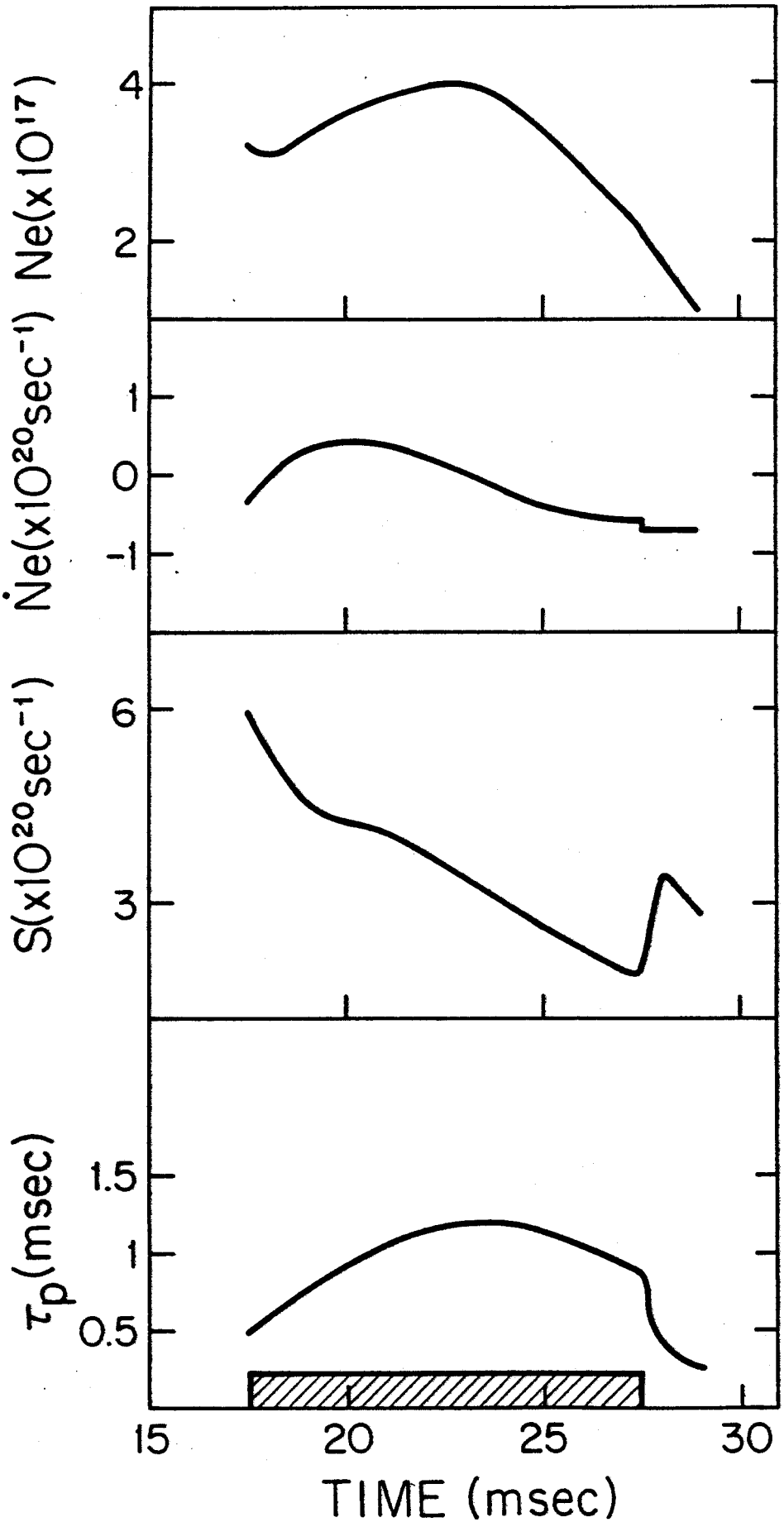
Ne(x10^17)
4
2
Ṅe(x10^20sec^-1)
1
0
-1
S(x10^20sec^-1)
6
3
τp(msec)
1.5
1
0.5
15
20
25
30
TIME (msec)

FIG. 3

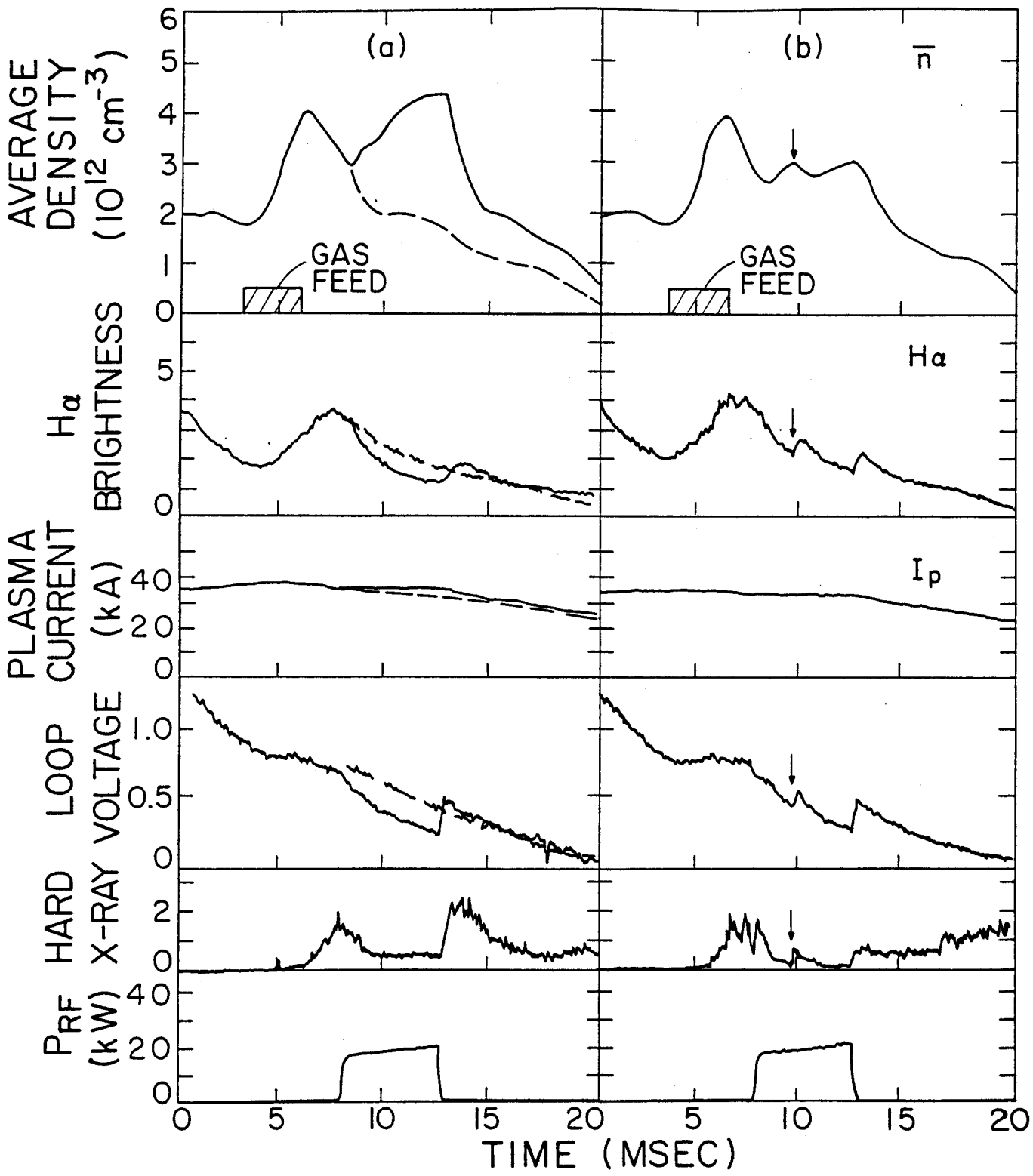
AVERAGE DENSITY (10^{12} cm^{-3})
(a)
(b)
$\bar{n}$
GAS FEED
GAS FEED
H_α BRIGHTNESS
H_α
PLASMA CURRENT (kA)
I_p
LOOP VOLTAGE
HARD X-RAY
P_{RF} (kW)
TIME (MSEC)

FIG. 4

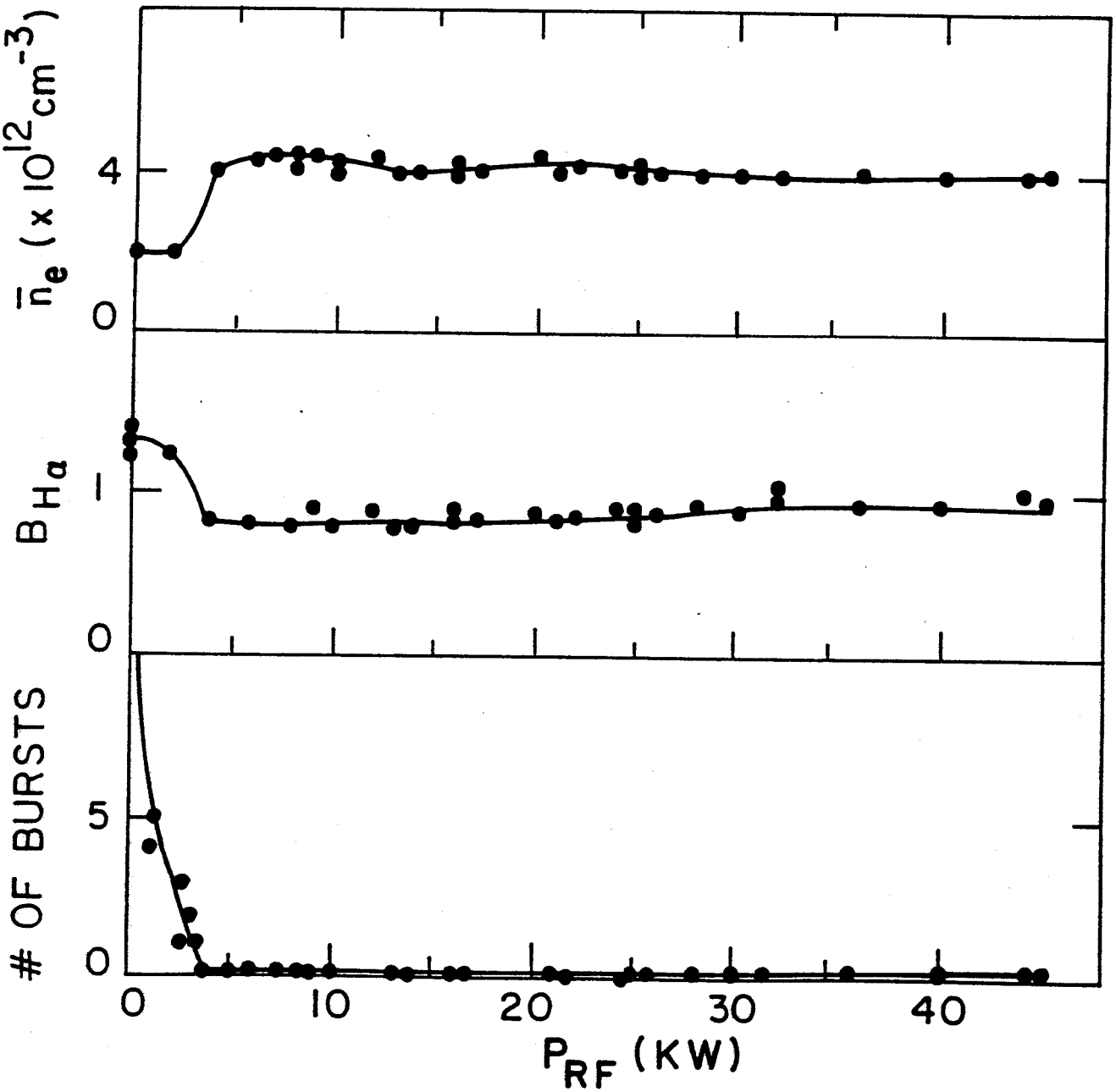

FIG. 5